

# Morphological Image Analysis of Quantum Motion in Billiards

J.S. Kole<sup>1</sup>, K. Michielsen<sup>2</sup> and H. De Raedt<sup>1</sup>

<sup>1</sup>*Institute for Theoretical Physics and Materials Science Centre,*

<sup>2</sup>*Laboratory for Biophysical Chemistry*

*University of Groningen, Nijenborgh 4, NL-9747 AG Groningen, The Netherlands*

Morphological image analysis is applied to the time evolution of the wavefunctions in quantum billiards. It is shown that the time average of the Euler characteristic of the probability density provides a quantitative measure to distinguish between classically integrable and non-integrable billiards.

The question whether quantum billiards show signatures of classical (non-)integrability has been of great interest [1–12]. One of the most studied problems in this context is that of two-dimensional billiards, on which we will focus our attention in this letter. In general, the distribution of energy-level separations of quantum billiards may be used to distinguish between classically integrable and non-integrable billiards [13], but exceptions are known [14,15].

In this letter, we present a new approach to relate quantum mechanical motion in billiards to the property of integrability of the corresponding classical problem. The time-evolution of the wavefunction is studied by morphological image analysis (MIA). MIA amounts to the characterization of the geometry and topology of any pattern or series of patterns by means of the so-called Minkowski functionals, known from integral geometry [16–18]. In two dimensions the Minkowski functionals correspond to the area, perimeter and Euler characteristic (the number of connected components minus the number of holes). We demonstrate that MIA provides a quantitative procedure for deciding, on the basis of the time-evolution of a quantum particle in a billiard, whether or not the billiard exhibits classical chaos.

MIA has proven to be a powerful tool in different fields where the description of patterns is important: Statistical physics, to describe the morphology of porous media and complex fluids; cosmology, to analyze the large scale distribution of matter in the universe; chemistry, to describe the morphology of patterns in reaction diffusion systems, and many other fields [19]. Furthermore, in the semi-classical limit the sum of exponentials of eigenfrequencies of a billiard-shaped drum can be written in terms of the Minkowski functionals of the billiard [20], and the Weyl hypothesis states that the number of energy levels up to an energy  $E$  can be written in a similar manner (see e.g. [21]).

Eigenstates of a quantum stadium may exhibit structure that corresponds to the classical orbits [22–24]. These structures, called scars, have been directly related to unstable periodic orbits [25–27], but their morphology has not been studied. Therefore it seems logical to use MIA to analyze the time-series of images of the probabil-

ity distribution of a quantum particle moving in billiards of different shape.

The application of MIA to the time evolution in quantum billiards is straightforward. We solve the time-dependent Schrödinger equation for a particle moving in a billiard by a stable and accurate numerical method [29]. For practical purposes the results obtained are exact. A time series of snapshots displaying the probability density can easily be extracted from this data. A collection of digital videos can be found in [30]. Each pattern of the time series is converted into a black-and-white picture by applying a threshold. Intensities below the threshold are considered to be part of the background, and intensities above the threshold value build up the objects. The result of applying a threshold of 10% to the probability density of a representative image is shown in Fig.1.

For each black-and-white picture we compute the Minkowski functionals using an algorithm described in Ref. [28] and analyze the behavior of the Minkowski functionals as a function of the control parameters, such as threshold, initial conditions of the wave packet, and shape of the billiard. We use Gaussian wave packets as initial states and study a variety of classically integrable and non-integrable billiards (See Fig.2). In our numerical work we express lengths in units of a fixed wavelength  $\lambda$  and rescale energy (and time, setting  $\hbar = 1$ ) such that a wave packet with average momentum  $2\pi/\lambda$  has an average kinetic energy of one [29].

In Figs.3 and 4 we present results that illustrate the typical behavior of Minkowski functionals as a function of time, keeping the threshold  $\theta$  fixed. Fig.3 shows the perimeter as a function of time for the two rectangularly shaped billiards (A,a), using a threshold  $\theta = 5\%$ . Billiard A (solid line) shows a behavior which is manifestly different from that of billiard a (dashed line): For times  $t > 100$  the solid line displays large fluctuations, in contrast to the dashed line. Other pairs of billiards (B,b, etc.) show very similar, characteristic fluctuations in the perimeter as a function of time (results not shown). Essentially the same behavior is found for the Euler characteristic  $\chi(t, \theta)$ . An example is given in Fig.4 for the case of billiards B and b and  $\theta = 15\%$ . The Euler characteristic  $\chi(t, \theta)$  is a global measure of the curvatures of the objects in the black-and-white image and provides direct quantitative information about the topology of the probability distribution (see [17, pp. 34,112 and 113]).

For each choice of the threshold  $\theta$ , the cumulative time average of the Euler characteristic approaches a constant

value

$$X(\theta) = \lim_{T \rightarrow \infty} X(T, \theta) \quad (1)$$

where

$$X(T, \theta) = \frac{\lambda^2}{AT} \int_0^T \chi(t, \theta) dt, \quad (2)$$

and  $A$  denotes the area of the billiard. A representative example of the behavior of the cumulative Euler characteristic is shown in Fig.5. In Fig.6 we plot the results for  $X(\theta)$ , for each of the billiards of Fig.2. As  $\theta$  approaches zero, the thresholded black-and-white picture becomes completely filled with black pixels, hence  $\lim_{\theta \rightarrow 0} X(\theta) = \lambda^2/A$ , for any image. Obviously, for  $\theta \rightarrow 0$ ,  $X(\theta)$  does not contain any useful information and for reasons of clarity we therefore omit data for  $\theta < 1$  in Fig. 6.

From Fig.6 it is clear that the  $X(\theta)$  curves form two clusters, depending on whether the system is classically integrable or not. In fact the maximum value of  $X(\theta)$  can be used to classify billiards according to their classical (non)integrability, as shown in Table I. The maxima for the classically integrable systems all lie in the range [0.97, 1.10], whereas the maxima for the classically non-integrable systems lie in the range [1.29, 1.38]. Further analysis shows that the maximum of  $X(\theta)$  changes with the energy of the wavepacket. This scaling behavior is trivially incorporated into the definition of  $X(\theta)$ . For a fixed energy of the wavepacket the results for  $X(\theta)$  are independent of other properties of the wavepacket. Calculations (not shown) for systems up to  $19\lambda \times 19\lambda$  demonstrate that  $\chi(t, \theta)$  scales linearly with the energy of the billiard, a dependence which could be easily incorporated into the definition of  $X(\theta)$ . Therefore we conclude that the scaling properties of  $X(\theta)$  can be employed to test for the (non)integrability of billiards.

To summarize: Morphological image analysis of the motion of a quantum particle in a billiard can be used to distinguish between classically integrable and non-integrable billiards.

We would like to thank the Dutch ‘Stichting Nationale Computer Faciliteiten’ (NCF) for their support and A. Lande for his critical reading of the manuscript.

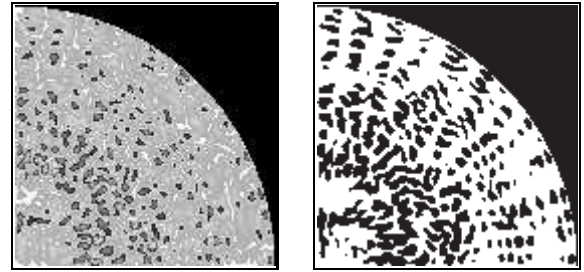


FIG. 1. The leftmost picture shows a snapshot of the probability density at  $t = 319$  (in dimensionless units, see text) in the case of a billiard in the form of a quarter circle. The picture on the right shows the result of thresholding the original image, using a threshold  $\theta = 10\%$ .

#### Classically Integrable Potentials



#### Classically Non-integrable Potentials

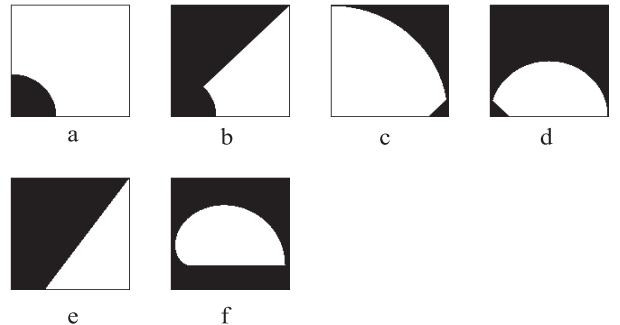


FIG. 2. The shapes of the various billiards studied. In most calculations the linear size of the square was taken to be  $13\lambda$ .

- [1] L. E. Reichl, *The Transition to Chaos* (Springer-Verlag, Berlin, 1992).
- [2] F. Haake, *Quantum Signatures of Chaos* (Springer-Verlag, Berlin, 1991).
- [3] M. C. Gutzwiller, *Chaos in Classical and Quantum Systems* (Springer-Verlag, Berlin, 1990).
- [4] O. F. de Alcantara Bonfim, J. Florencio and F. C. Sá Barreto, Phys. Rev. E **58**, 2693 (1998).
- [5] H. Wu and D. W. L. Sprung, Phys. Lett. A. **261**, 150 (1999).
- [6] O. Bohigas, M. Giannoni and C. Schmidt, Phys. Rev. Lett. **52**, 1 (1984).
- [7] R. Aurich, J. Bolte, and F. Steiner, Phys. Rev. Lett. **73**, 1356 (1994).
- [8] R. Aurich, A. Bäcker and F. Steiner, Int. J. Mod. Phys. B **11**, 805 (1997).
- [9] J. A. Vergés and E. Louis, Phys. Rev. E **59**, R3803 (1999).
- [10] G. Casati and T. Prosen, Phys. Rev. E **59**, R2516 (1999).
- [11] V. Lopac, I. Mrkonjić and D. Radić, Phys. Rev. E **59**, 303 (1999).
- [12] S. Ree and L. E. Reichl, Phys. Rev. E **60**, 1607 (1999).
- [13] S. W. McDonald and A. N. Kaufman, Phys. Rev. Lett. **42**, 1189 (1979).
- [14] J. Zakrzewski, K. Dupret and D. Delande, Phys. Rev. Lett. **74**, 522 (1995).
- [15] P. Crehan, J. Phys. A: Math. Gen. **28**, 6389 (1995).

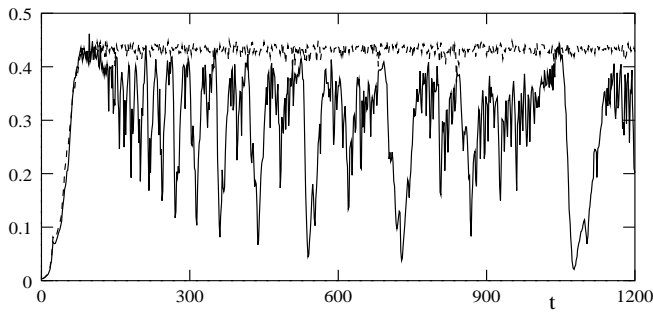


FIG. 3. Perimeter (in pixels) as function of time, normalized to the area of the billiard (in pixels). Time is measured in dimensionless units (see text). Solid line: Billiard A. Dashed line: Billiard a.

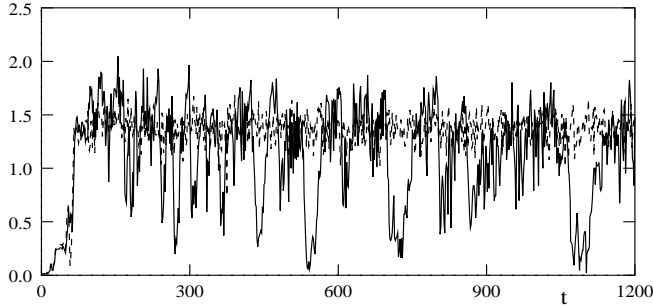


FIG. 4. Euler characteristic  $\chi(t, \theta)$  as function of time, normalized to the area of the billiard. Solid line: Billiard B. Dashed line: Billiard b.

- [16] H. Hadwiger, *Vorlesungen über Inhalt, Oberfläche und Isoperimetrie* (Springer-Verlag, Berlin, 1957).
- [17] L. A. Santaló, *Integral Geometry and Geometric Probability* (Addison-Wesley, Reading, Massachusetts, 1976).
- [18] D. Stoyan, W. S. Kendall and J. Mecke, *Stochastic Geometry and its Applications* (Akademie Verlag, Berlin, 1989).
- [19] K. R. Mecke, Int. J. Mod. Phys. B **12**, 861 (1998).
- [20] M. Kac, Amer. Math. Monthly **73**, 1 (1966).
- [21] H. P. Baltes and E. R. Hilf, *Spectra of finite systems* (Bibliographisches Institut, Mannheim, 1976).
- [22] S. W. McDonald, Lawrence Berkeley Lab. Report LBL-14837 (1983).
- [23] R. D. Taylor and P. Brumer, Faraday Discuss. Chem. Soc. **75**, 170 (1983).
- [24] E. J. Heller, Phys. Rev. Lett. **53**, 1515 (1984).
- [25] E. B. Bogomolny, Physica D **31**, 169 (1988).
- [26] M. V. Berry, Proc. R. Soc. Lond. A **423**, 219 (1989).
- [27] M. Feingold *et al.*, Phys. Lett. **A146**, 199 (1990).
- [28] K. Michielsen, H. De Raedt, subm. to Comp. Phys. Com.
- [29] H. De Raedt and K. Michielsen, Comp. in Phys. **8**, 600 (1994).
- [30] <http://rugth30.phys.rug.nl/compphys/chaos.htm>.

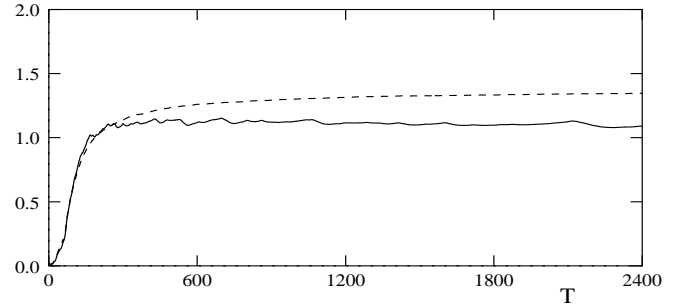


FIG. 5.  $X(T, \theta)$  as function of time. Solid line: Billiard B. Dashed line: Billiard b.

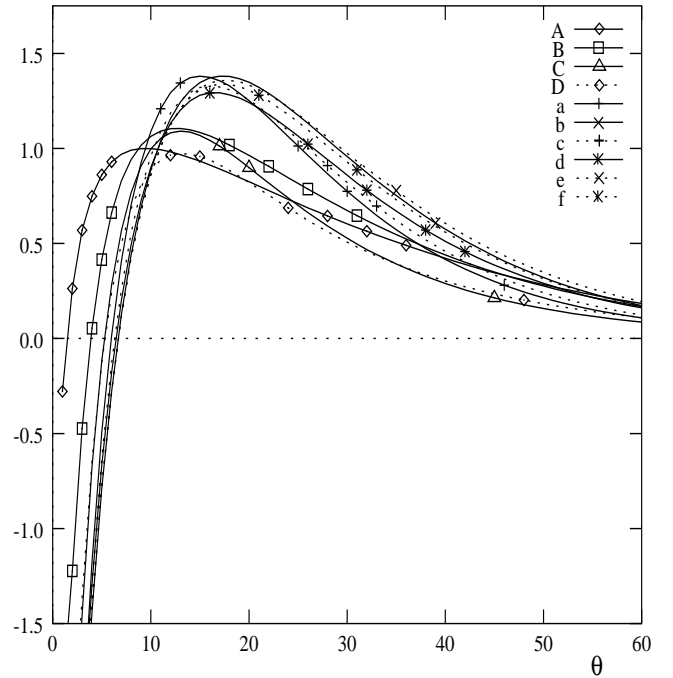


FIG. 6.  $X(\theta)$  as function of the threshold  $\theta$  (in percent), for all billiards shown in Fig. 2.

Billiard	$\theta$	$X$
A	10	1.00
B	13	1.10
C	13	1.09
D	13	0.97
a	15	1.38
b	17	1.38
c	16	1.33
d	17	1.29
e	18	1.36
f	17	1.34

TABLE I. The maximum value of  $X(\theta)$  for each billiard.